A COMPREHENSIVE MODELLING APPROACH OF FATIGUE INDUCED CRACKING IN CARBON FIBRE REINFORCED LAMINATES AT DIFFERENT STRESS RATIOS

G. Just, I. Koch and M. Gude

Institute of Lightweight Engineering and Polymer Technology, Technische Universität Dresden, Holbeinstraße 3, 01307 Dresden, Germany
Email: gordon.just@tu-dresden.de, ilja.koch@tu-dresden.de, maik.gude@tu-dresden.de
Web Page: http://www.tu-dresden.de/ing/maschinenwesen/ilk

Keywords: CFRP, Fatigue, Fracture, Inter fibre failure, Load reversal, Stress ratio

Abstract
The work presented here is part of a collaborative project of Polymer Composites (TU Hamburg-Harburg), IKV at RWTH Aachen, ILK (TU Dresden) and ISD (Leibniz Universität Hannover) funded by the German Research Foundation (DFG). It focusses the analysis of multi-scale damage of endless fibre reinforced composites under reversed cyclic loading. Carbon fibre reinforced cross-ply laminates were subjected to fatigue loading at four different stress ratios. The evolution of crack density and the crack angles were recorded throughout the experiments by optical microscopy. It was found that the crack density evolution depends on the present stress ratio and amplitude, but the crack angles were barely effected by the stress ratio. Conclusively, a finite fracture mechanics approach was established, to account for load reversals in strain energy release rate calculations.

1. Introduction

Fibre reinforced composites in structural applications are used for wind turbines since many years and are getting increasingly attention in automotive and aircraft industry. They usually exhibit complex loading situations, which are characterised by multiaxial loading conditions in terms of combined normal and shear loads. Furthermore, composites are often subjected to fatigue loading with changing load direction vector, resulting in tension and/or compression loadings. The most detrimental effect of these loading situations has been found in tension-compression loads comprising repeated load reversals, what is expressed in terms of a more pronounced accumulation of inter fibre cracks and elevated stiffness degradation [1, 2]. High efforts in research have been put into the development of suitable damage models that describe fatigue damage evolution. Current approaches aim on a physically based description of the mechanisms of inter fibre failure and their influence on laminate properties. For this purpose, microscopic composite failure is modelled explicitly by means of finite element (FE) analysis and its effects on ply-properties are computed. These findings were generalised for tension loading at any applied stress level and used in conjunction with semi-analytical models to describe damage evolution in composites with off-axis plies, as recently presented by GLUD et al. [2].

It is therefore of high interest to analyse the effect of load reversals on the evolution of inter fibre cracks in composite laminates with respect to the underlying mechanisms. Load reversals might change the amount of cracks forming in fatigue experiments as well as affect the crack angle due to different fracture modes that are activated. Whereas in pure tension or compression loading only one fracture mode is active the situation changes in case of negative stress ratios. Here, the active fracture mode changes within every cycle and it is not obvious from the beginning, which fracture mode will prevail or if they affect each other.

Within the framework of a collaborative project, dealing with micro- and macroscopic analysis and description of fatigue damage under reversed loading, an experimental study was conducted to fortify the efforts made to clarify the influence of alternating loads on composite damage behaviour.

2. Materials and methods

The experiments in this study were conducted with the commercially available fibre T700S from TORAYCA® and resin system Araldite LY556, Hardener HY 917 and Accelerator DY 070 in a mixing ratio of 100:90:1 provided by HUNTSMAN LLC®. Unidirectional ($[0_{11}]$) and cross-ply ($[0_2/90_7/0_2]$) lay-ups with a nominal fibre volume fraction of 60 % were made by filament winding followed by resin transfer moulding. The curing and post-curing procedures were performed according to the manufacturers recommendations. Finally, aluminium end tabs were glued to the composite plates and the specimens were cut to size with an abrasive cutting machine. Specimen preparation was finished by edge polishing. The final dimensions of the flat strip specimens are 190 mm × 25 mm × 2 mm (length × width × thickness).

Elastic properties of the UD-specimens were determined by at least four specimens parallel and transverse to the fibre direction, according to DIN EN ISO 527 [3]. The shear modulus G_{12} was measured according to ASTM D 7078 [4] by V-notched rail shear (VNRS) experiments parallel to the fibres. Coefficients of thermal expansion (CTE) α_{ij} have been determined by dilatometer measurements (DIN 53752 [5]) and ply thicknesses (for laminates) were measured by optical microscopy. The results of the material characterisation are summarised in table 1.

Table 1. In-plane elastic material properties of T700S/LY556 UD-ply.

Value (Units)	E_1 (GPa)	E_2 (GPa)	ν_{12} (-)	G_{12} (GPa)	α_{11} (10^{-6}/K)	α_{22} (10^{-6}/K)	t_0 (µm)	t_{90} (µm)
Mean	129.4	8.05	0.317	3.92	0.5	38	184.2	178.5
Std. dev.	5.4	0.44	0.007	0.19	-	-	7.3	7.6

Fatigue experiments were performed on a servo-hydraulic testing machine (Instron 8801) equipped with mechanical wedge grips. Tests were performed in load control accompanied by strain ($L_0 = 50$ mm) and LVDT measurements perpendicular to the loading direction to monitor possible specimen bending in compression loading. All experiments were performed in standard atmosphere at $\vartheta_{RT} = 23$°C and 50 % r.H. inside a climate chamber. The specimens were regularly unmounted from the testing machine and inspected at the specimen edges to analyse crack formation as well as delamination growth. Fatigue experiments were performed for the chosen load ratios $R = \{0, -1, -3.26, \infty\}$ at a maximum stress of $\sigma_{xx,o}^{lam} = 105$ MPa for pure tension and tension-compression tests and $\sigma_{xx,u}^{lam} = -380$ MPa for pure compression fatigue loading.

3. Experimental results

3.1. Determination of residual stresses

Due to the chosen cross-ply lay-up and the anisotropy of the CTEs it is vital to pay attention to the formation of residual stresses within the layers, because they have serious influence on stress ratios within the layers, as discussed later in section 4. The mismatch of CTEs in layers oriented along and transverse to the loading direction leads to a significant amount of residual stresses after the curing and post-curing procedures resulting from cooling and shrinkage processes. Hence, determination of residual stresses is a painstaking task and accomplished here by crack opening displacement (COD) measurements, assuming that both thermal and chemical shrinkage contribute to the COD. However, separation of the contributions is neither possible nor intended here.

The separation of crack surfaces has been measured by image analysis in MATLAB® from high resolution microscopic images of the first two cracks in the laminate after 5000 cycles at a maximum stress $\sigma_{xx,o}^{lam} = 95$ MPa and fully reversed loading ($R = -1$), stitched together from 8-9 single images with 500-fold magnification. Simultaneously, FE-models were set up, to determine the corresponding

temperature change $\Delta T = -110$ K, which induces the same COD within FE-calculations as observed from experiments [6]. The analysed cracks and the results of the experimental measurements as well as FE-calculations are shown in fig. 1 (a) – (c).

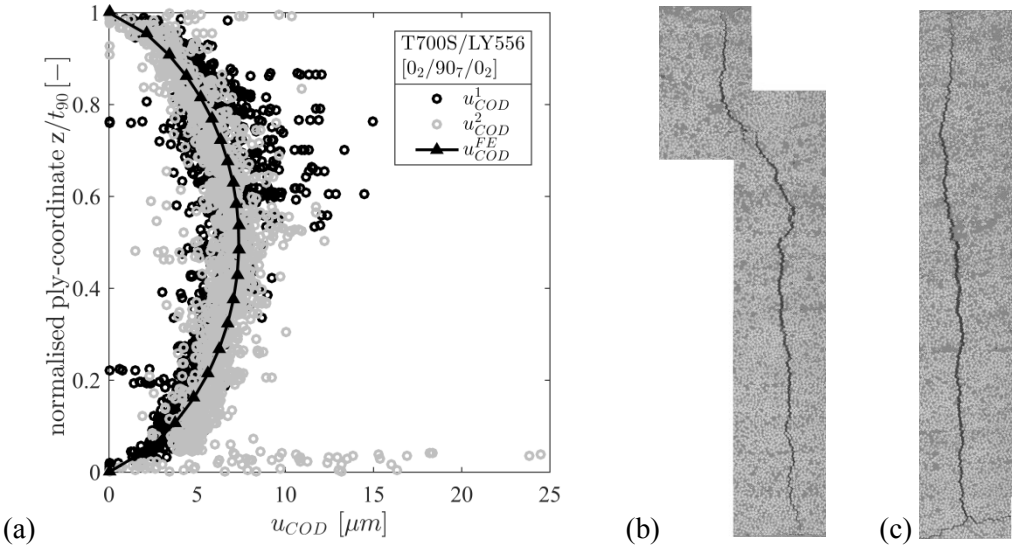

Figure 1. Determination of residual crack opening displacement (COD) in the 90°-ply of a cross-ply laminate after fatigue loading for n = 5000 cycles with $\sigma^{lam}_{xx,o} = 95$ MPa at R = -1 (a) and microscopic images of the analysed cracks 1 (dark circles) (b) and 2 (pale circles) (c) after unmounting from the testing machine.

From FE-calculations the residual stresses in the 90°- and 0°-ply have been determined to $\sigma^{90}_{res} = [-15.9\ 27.2\ 0]^T$ and $\sigma^{0}_{res} = [-43.2\ 27.9\ 0]^T$, respectively and the mean crack opening was found to be $\tilde{u}_{COD} \approx 5.5$ µm (averaged about both cracks), implying an residual crack opening after unloading.

3.2. Evolution of fatigue damage

Manual crack counting along an inspection distance of $L_c = 50$ mm at the specimen edges has been performed for one specimen per load ratio by optical microscopy and the crack density $c = \sum n/L_c$, with n the number of observed cracks, is determined as the mean from both specimen edges. Furthermore, the angles inclined by the observed cracks and the z-axis (thickness direction) have been reported, as seen in fig. 2 (a) and (b), respectively.

Regarding fig. 2 (a) it comes clear that, at constant amplitude loading with different R-ratios, damage evolution in terms of the formation of inter fibre cracks is depending on the applied stress ratio and is most tremendous for reversed loadings ($R = -1$ and $R = -3.26$). The specimen fatigued at $R = -3.26$ failed after $n = 210000$ cycles, due to delamination growth, subsequent buckling of the 0°-ply and final compression failure of the whole specimen. Surprisingly, the compression loaded specimen ($R = \infty$) also developed a significant number of cracks, but crack evolution appears to be delayed and distinctly slower than for other stress ratios.

On the contrary, crack angle analysis does not reveal substantial differences between the stress ratios, as depicted in fig. 2 (b). In all cases the mean crack angle inclined with the thickness direction is $\theta_{fr} \approx 5°$. However, there is a noticeable higher scatter in case of load reversal, but comparable mean values and scatter bands are observed for $R = 0$ and $R = \infty$, which is remarkable, because the activated fracture modes should be different and a change of the crack angles was expected. The results clarify, that, for the given test conditions and applied loadings, most of the cracks are aligned perpendicular to the loading direction regardless of the applied stress ratio.

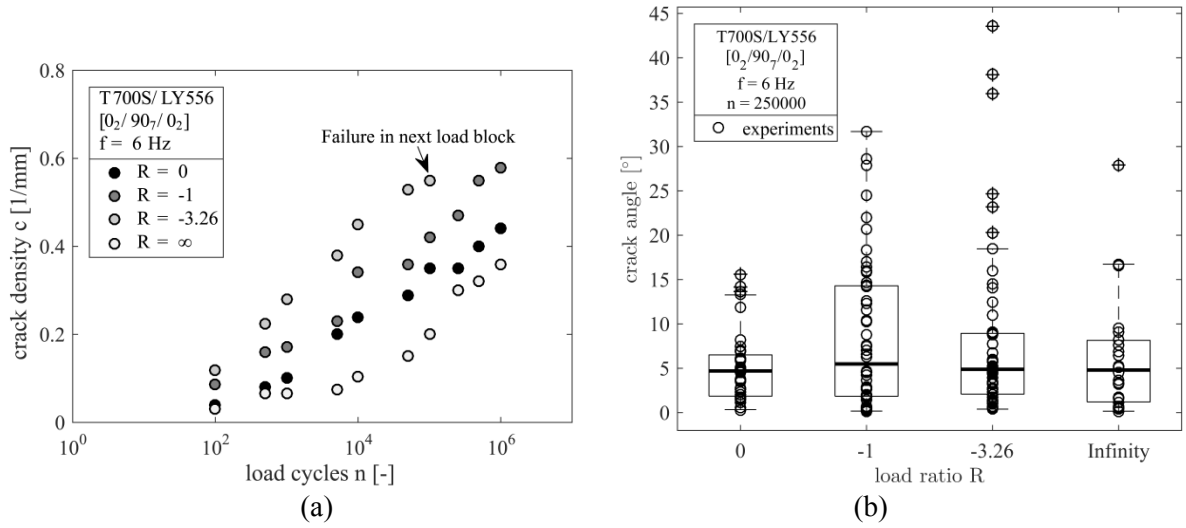

Figure 2. Crack density evolution in constant amplitude fatigue experiments (a) and crack angles as observed by optical microscopy for different R-ratios after $n = 250000$ cycles (b).

4. Modelling approach

4.1. Influence of residual stresses on cyclic stress state and stress ratio

From the experimental findings it is concluded, that the macroscopically applied stress ratio differs from the stress ratio, which is actually present in the 90°-layer. Assuming that the residual stresses act like superimposed mean stress the local stress ratio in the 90°-layer of an undamaged laminate can be calculated in terms of

$$R^{90} = \frac{\left(\sigma_m + \frac{E_{xx}^{lam}}{E_2^{90}}\sigma_{2,res}^{90}\right) - \sigma_a}{\left(\sigma_m + \frac{E_{xx}^{lam}}{E_2^{90}}\sigma_{2,res}^{90}\right) + \sigma_a}, \tag{1}$$

with the macroscopic mean stress σ_m and amplitude σ_a, the axial laminate modulus E_{xx}^{lam} and the modulus E_2^{90} and residual stress $\sigma_{2,res}^{90}$ transverse to the fibres in the 90°-layer, respectively. Hence, the local stresses acting within the 90°-layer are shifted towards tension loading and the local stress ratio is significantly altered, as seen from fig. 3 (a). In case of macroscopically loading at $R = 0$ and $R = -1$ the cyclic stresses within in the 90°-layer are purely pulsating tension loads, the compression part at $R = -3.26$ is heavily decreased and even the macroscopically compression load at $R = \infty$ shows severe tension load contributions in the 90°-layer cyclic stresses. Following these considerations, it is inferred that cracks forming under macroscopic compression loading, are also initiated by tensile loads – in this case pulsating residual stresses, which are supressed by compression loads and built up again when the specimens are macroscopically unloaded. To account for this tension-compression asymmetry, a simple approach to separately calculate the tension and compression contributions to the strain energy release rates (SERR) in case of crack formation is made in the following.

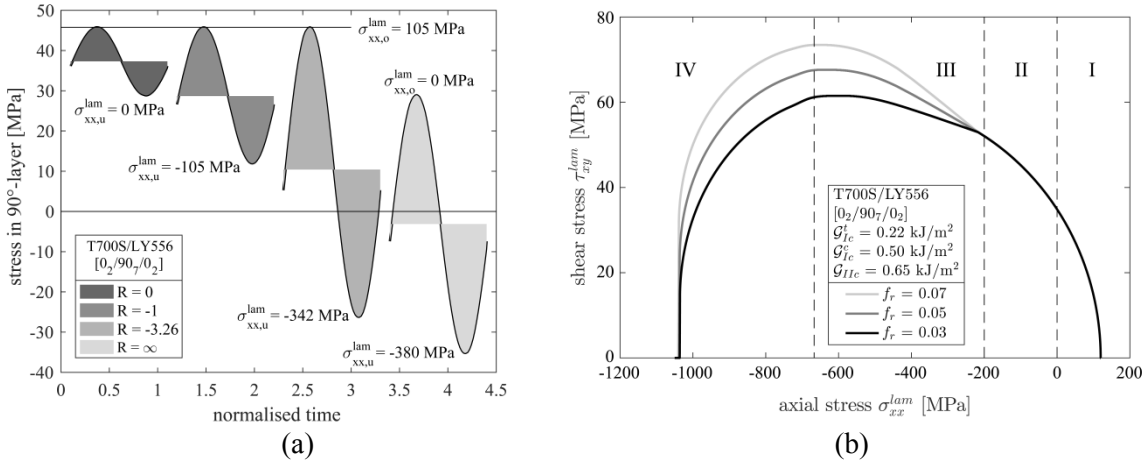

Figure 3. Influence of residual stresses on the local stress ratio in an embedded 90°-layer subjected to axial cyclic loading at several macroscopic stress ratios (a) and calculated fracture curve for a 90°-layer within a cross-ply laminate under combined axial and shear loading (b).

4.2. Calculation of strain energy release rate in tension and compression

Using the analytical model published by MAYUGO et al. [7] the SERR can be calculated based on the elastic properties of the laminate and the applied tension and shear loads. They further point out to be able to calculate the SERR in case of compression loads and off-axis fibre orientation, except for 90°-layers, meaning the cracks are formed by shear stresses, which correspond to mode II crack formation. Further details of the model can be found in [7].

To account for fracture in the 90°-layer under compression loads, the crack angle within the 90°-layer is introduced into the model formulation with respect to the effect of compressive stresses on the mode II fracture toughness [8]. It is hence assumed, that the increase of mode II fracture toughness can be explained by internal material friction, which is understood as a friction stress resulting from the normal compression stress active on the fracture plane acting "against" the applied shear stress. The modified equations for the SERR under load control in mode I and II from [7] then read as

$$\mathcal{G}_I = -\left(\frac{1}{E^{lam}_{xx}(L)} - \frac{1}{E^{lam}_{xx}\left(\frac{L}{2}\right)}\right)\frac{cos(\theta_{fr})Lh}{t^{90}}\left(\sigma^{lam}_{xx}\right)^2 , \tag{2}$$

$$\mathcal{G}_{II} = -\left(\frac{1}{G^{lam}_{xy}(L)} - \frac{1}{G^{lam}_{xy}\left(\frac{L}{2}\right)}\right)\frac{cos(\theta_{fr})Lh}{t^{90}}\left(\tau^{lam}_{xy}\right)^2, \tag{3}$$

where L denotes the current crack spacing, h is the total laminate thickness, θ_{fr} the fracture angle inclined with the laminate thickness direction, t^{90} the thickness of the 90°-layer and the corresponding laminate stresses

$$\sigma^{lam}_{xx} = \begin{cases} \sigma^{lam}_{xx} + \dfrac{E^{lam}_{xx}}{E^{90}_2}\sigma^{90}_{2,res} & \text{(tension)}, \\ \left(\sigma^{lam}_{xx} + \dfrac{E^{lam}_{xx}}{E^{90}_2}\sigma^{90}_{2,res}\right)\sin(\theta_{fr}) & \text{(compression)}, \end{cases} \tag{4}$$

$$\tau_{xy}^{lam} = \begin{cases} \tau_{xy}^{lam} + \dfrac{G_{xy}^{lam}}{G_{12}^{90}}\tau_{12,res}^{90} & \text{(tension) and} \\ \left(\tau_{xy}^{lam} + \dfrac{G_{xy}^{lam}}{G_{12}^{90}}\tau_{12,res}^{90}\right) - \left|\mu_r\left(\sigma_{xx}^{lam} + \dfrac{E_{xx}^{lam}}{E_2^{90}}\sigma_{2,res}^{90}\right)\cos(\theta_{fr})\right| & \text{(compression)} \end{cases} \tag{5}$$

with the internal material friction parameter μ_r. Under combined shear and tension/compression loadings the fracture behaviour of the embedded transverse layer preserves a mixed-mode character and requires a mode-mix criterion to analyse composite microcracking. The mode-mix criterion from HAHN [9] used in energy formulation [7] is applied to calculate the critical SERR for multiaxial loading conditions and takes the following form

$$\mathcal{G}_c = \mathcal{G}_{IIc}\frac{(1-\zeta)}{2}\frac{(\mathcal{G}_{Ic}-\mathcal{G}_{IIc})^2}{\mathcal{G}_{Ic}}\left(1-\sqrt{1+\frac{4}{(1-\zeta)}\frac{\mathcal{G}_{Ic}\mathcal{G}_{IIc}}{(\mathcal{G}_{Ic}-\mathcal{G}_{IIc})^2}}\right), \tag{6}$$

with the mode-mix ratio defined as $\zeta = \mathcal{G}_{II}/(\mathcal{G}_I + \mathcal{G}_{II})$. Please note, that the value of the critical mode I fracture toughness $\mathcal{G}_{Ic}$ depends on the applied loading direction. Fracture curves for T700S/LY556 material are exemplarily shown in fig. 3 (b). The friction parameter μ_r directly affects the amount of shear stresses necessary to introduce inter fibre cracks in the cross-ply laminate and has to be determined experimentally. The compression strength of the laminate is assumed to be coincident with the failure strain of the 0°-ply leading to a mode I SERR in compression of $\mathcal{G}_{Ic}^{c} = 0.5$ kJ/m², whereas the tensile strength is taken as the stress at crack initiation and was determined to be $\sigma_{xx,ini}^{lam} = 120$ MPa corresponding to a SERR in tension of $\mathcal{G}_{Ic}^{t} = 0.22$ kJ/m². The mode II SERR $\mathcal{G}_{IIc} = 0.65$ kJ/m² is taken from the literature [10] for a comparable material.

Regarding fig. 3 (b), there are four distinct regions characterising the fracture curve. Region I represents the stress range with tension failure of the transverse ply from a macroscopically as well as a ply-stress based view, with the fracture angle $\theta_{fr}^{I} = 0°$. Within region II, the applied loads are compressive, but the ply-stresses are still tension stresses due to residual stresses. The corresponding fracture angle does not change ($\theta_{fr}^{II} = 0°$). Failure in region III is dominated by shear stresses accompanied by rising compressive stresses in the 90°-layer. Therefore increasing fracture angles $\theta_{fr}^{III} > 0°$ have to be expected. Due to the relatively low amount of axial compressive stresses the fracture angles are assumed to be small. The influence of compressive stresses rises with increasing compression loads in region IV and the fracture criterion is fulfilled without the need for high shear stresses. The expected fracture angles also increase, thus $\theta_{fr}^{IV} > \theta_{fr}^{III} > 0°$. Consequently, the calculation of the appropriate SERR premises the determination of the active fracture mode.

It should be noted that in terms of the proposed approach, it is possible to calculate the SERRs for mode I in tension and compression as well as mode II from macroscopically applied loads – solely the residual stresses within the 90°-layer have to be determined, which can be easily done by means of classical laminated plate theory (CLT). In terms of fatigue experiments, the SERRs for alternating loads can now be computed with respect to the tensile and compression load contributions to derive the appropriate PARIS-like crack density growth curves from the fatigue experiments depicted in fig. 2 (a).

5. Conclusion

The present study focusses on the analysis of the effect of stress ratio on composite microcracking with special attention to reversed loading. Carbon fibre reinforced composite laminates were fatigued at four different stress ratios for up to one million cycles. It has been found, that the microcracking process is significantly altered by the chosen stress ratio. Experimental examination of the crack

opening displacement of cross-ply laminates after unloading revealed a residual COD, which was attributed to the presence of residual stresses. By means of optical microscopy and associated FE-calculations the residual stresses were determined from the CODs and used to compute local stress ratios within the transverse layer. Due to the present residual stresses, the mean stress in the 90°-layer is shifted towards tension loading, significantly changing the local stress ratio. With that said, the microcrack formation as observed in the experiments can be interpreted as a tensile stress driven cracking process with varying amplitudes. This is further encouraged by the observation of mainly perpendicular cracks even under (macroscopically) pure compression loading. Finally, a finite fracture mechanics approach has been proposed to appropriately compute the SERR under tension or compression mixed-mode loading. The approach is capable of describing fracture curves for in-plane loading and introduces only one additional model parameter to account for internal material friction.

Future work will focus on the application of the modelling approach to available fatigue data and the derivation of suitable mathematical description for the stress ratio effect on fatigue crack growth.

Acknowledgements

The authors gratefully acknowledge the financial support granted by the German Research Foundation (DFG) within the project FATIGUE at TU Dresden (GU 614/10-1), as well as the collaboration and scientific discussions with the colleagues from TU Hamburg-Harburg, IKV Aachen and ISD Hannover.

References

[1] E.K. Gamstedt and B.A. Sjögren. Micromechanisms in tension-compression fatigue of composite laminates containing transverse plies. *Composites Science and Technology*, 59:167–178, 1999.

[2] J.A. Glud, J.M. Dulieu-Barton, O.T. Thomsen and L.C.T. Overgaard. Fatigue damage evolution in GFRP laminates with constrained off-axis plies. *Composites Part A: Applied Science and Manufacturing,* 95:359–369, 2017.

[3] N.N. *DIN EN ISO 527 – Kunststoffe – Bestimmung der Zugeigenschaften*, 2012.

[4] N.N. *ASTM D 7078 – Standard Test Method for Shear Properties of Composite Materials by V-Notched Rail Shear Method*, 2005.

[5] N.N. *DIN 53752 – Prüfung von Kunststoffen – Bestimmung des thermischen Längen-ausdehnungskoeffizienten*, 1980.

[6] I. Koch, G. Just and M. Gude. Discussions on the influence of residual stresses to the fatigue of layered polymer composites. *Proceedings of the 2nd International Symposium on Multiscale Experimental Mechanics: Multiscale Fatigue, Lyngby, Denmark,* November 8-9 2017.

[7] J.A. Mayugo, P.P. Camanho, P. Maimí and C.G. Dávila. Analytical Modelling of Transverse Matrix Cracking of $[\pm\theta/90_n]_s$ Composite Laminates under Multiaxial Loading. *Mechanics of Advanced Materials and Structures*, 17:237–245, 2010.

[8] Q. Bing and C.T. Sun. Effect of compressive transverse normal stress on mode II fracture toughness in polymeric composites. *International Journal of Fracture*, 145:89–97, 2007.

[9] H.T. Hahn. A mixed-mode fracture criterion for composite materials. *Journal of Composites, Technology and Research*, 5:26–29, 1983.

[10] A. Kaddour, M. Hinton, P. Smith and S. Li. Mechanical properties and details of composite laminates for the test cases used in the third world-wide failure exercise. *Journal of Composite Materials,* 47:2427–2442, 2013.